Journal of Applied Physics

Enhanced converse flexoelectricity in piezoelectric composites by coupling topology optimization with homogenization

Cite as: J. Appl. Phys. **129**, 245104 (2021); https://doi.org/10.1063/5.0051062
Submitted: 22 March 2021 . Accepted: 09 June 2021 . Published Online: 22 June 2021

X. Chen, J. Yvonnet, H. S. Park, and S. Yao

Note: This paper is part of the Special Topic on Trends in Flexoelectricity.

This paper was selected as an Editor's Pick

AIP Publishing

Journal of Applied Physics ARTICLE scitation.org/journal/jap

Enhanced converse flexoelectricity in piezoelectric composites by coupling topology optimization with homogenization

Cite as: J. Appl. Phys. **129**, 245104 (2021); doi: 10.1063/5.0051062
Submitted: 22 March 2021 · Accepted: 9 June 2021 ·
Published Online: 22 June 2021

X. Chen,[1,2] J. Yvonnet,[2,a)] H. S. Park,[3] and S. Yao[1]

AFFILIATIONS

[1]Key Laboratory of Traffic Safety on Track, Ministry of Education, School of Traffic and Transportation Engineering, Central South University, Changsha 410075, China
[2]MSME, Gustave Eiffel University, CNRS UMR 8208, F-77454 Marne-la-Vallée, France
[3]Department of Mechanical Engineering, Boston University, Boston, Massachusetts 02215, USA

Note: This paper is part of the Special Topic on Trends in Flexoelectricity.
a)Author to whom correspondence should be addressed: julien.yvonnet@univ-paris-est.fr

ABSTRACT

We demonstrate that large apparent converse flexoelectric properties can be obtained in piezoelectric composites using theoretical approaches. To do so, we first present a numerical homogenization method accounting for all electromechanical terms related to strain and the electric field gradient. We then evaluate the coefficients of the model by numerical simulations on periodic piezoelectric composites. After combining the homogenization approach with topology optimization to enhance the converse properties of the composite, we present numerical results that reveal that the apparent converse flexoelectric coefficients, as well as those associated with the higher order coupling terms involving the electric field gradient, are of the same order as the direct flexoelectric properties of the local constituents. These results suggest that both converse and higher order electromechanical coupling effects may contribute strongly to the flexoelectric response and properties of piezoelectric composites. Finally, we show that it is theoretically possible to obtain optimized designs of composites with apparent converse flexoelectric properties 1–2 orders of magnitude larger than ones obtained with naïve guess designs.

I. INTRODUCTION

Direct flexoelectricity is a phenomenon whereby electrical polarization can be induced by generating a strain gradient or an inhomogeneous deformation on the sample. This so-called direct flexoelectric effect has been widely studied in ferroelectric materials[1] and complex oxide ceramics[2–5] as the effects are much larger in these materials but more recently, in several polymers[6,7] as well as in biological membranes.[8] Kogan[9] formulated the first phenomenological theory of flexelectricity and estimated the range of values for flexoelectric coefficients. Tagantsev[10] developed a microscopic theory for the bulk contributions using the rigid-ion approximation as well as a phenomenological description. Promising applications of direct flexoelectricity have been studied like the possibility of building a piezoelectric composite with nonpiezoelectric materials,[11–16] energy harvesters,[17,18] or new field-gradient-based sensors.[19] In Ref. 20, it was demonstrated that piezocomposites with designed microstructures could exhibit apparent enhanced flexoelectric properties of the same order as oxide ceramics or ferroelectrics.

In contrast to direct flexoelectricity, the converse flexoelectric effect describes a mechanical strain induced by an electric field gradient. Studies on converse flexoelectricity have only emerged very recently and remain limited.[2,21–27] As noted in Ref. 21, understanding and modeling of the converse flexoelectric effect may help not only in understanding unexplained enhanced piezoelectricity in dielectrics and ferroelectrics but also in designing and developing new electromechanical devices. The inverse and converse flexoelectric effects have been experimentally demonstrated by applying a voltage to a capacitor and measuring its bending[13,28] and by applying a voltage to a truncated pyramid so as to generate an

inhomogeneous electric field, thus allowing the sample to deform.[1,2,29] Fu *et al.*[2] reported experimental observations of the converse flexoelectric effect in a $Ba_{0.67}Sr_{0.33}TiO_3$ (BST) trapezoidal ceramic block under an inhomogeneous electric field. In Ref. 26, Shu *et al.* measured converse flexoelectric coefficients in BST. Wang *et al.*[21] showed the important role of converse flexoelectricity on asymmetric structures surrounding domain walls in $PbTiO_3$. Abdollahi *et al.*[23] demonstrated a large effective piezoelectric response in nonpiezoelectric materials such as $SrTiO_3$ and demonstrated that converse flexoelectricity may have non-negligible effects in thin films. In Ref. 24, converse flexoelectric effects were generated by the design permittivity gradient with BST powder and a substrate. Shen and Chen[25] demonstrated the converse flexoelectric effect in a lead zirconate titanate microbeam. Tian *et al.*[22] provided explicit solutions for physical fields around a microhole with simultaneous consideration of the strain gradient elasticity, direct flexoelectricity, and converse piezoelectricity. Shu *et al.*[27] provided relationships between converse and direct flexoelectric coefficients. Mawassy *et al.*[30] developed an extended flexoelectric framework involving electric field gradient coupling terms and proposed a finite element framework for their evaluation. Finally, Wang *et al.*[31] conducted an extensive survey on theoretical and experimental approach to determine the direct and converse flexoelectric values in several ferroelectric oxides.

Therefore, two key issues related to flexoelectricity that we attempt to resolve in the present work are, first, to enable calculations of the converse flexoelectric effect for general situations and, second, to determine the importance of higher order electric field gradient effects on the flexoelectric response. Therefore, in this paper, we employ a homogenization method to predict the apparent converse flexoelectric properties of piezoelectric composites. Following our previous work,[20] where the homogenized direct flexoelectric properties were provided, we propose here an extended effective model accounting for all coupling terms between strain, electric field, strain gradient, and electric field gradient. We provide expressions for all of the coupling tensors in a fully anisotropic context and demonstrate via numerical examples that these coupling terms, as well as the converse flexoelectric effect, are of the same order as the direct flexoelectric constants of the constituent materials. Finally, we combine this model with topology optimization to obtain tailored microstructures with converse flexoelectric properties that exceed those obtained with naïve guesses.

II. AN EXTENDED FLEXOELECTRIC MODEL

We define the total energy density $\overline{W}$ for an electromechanical system where all couplings between strains $\overline{\varepsilon}$, stress $\overline{\sigma}$, electric field $\overline{E}$, strain gradient $\overline{\nabla\varepsilon}$, and electric field gradient $\overline{\nabla E}$ are taken into account,

$$\begin{aligned}\overline{W} = &\frac{1}{2}\overline{C}_{ijkl}\overline{\varepsilon}_{ij}\overline{\varepsilon}_{kl} - \frac{1}{2}\overline{\alpha}_{ij}\overline{E}_i\overline{E}_j - \overline{e}_{ijk}\overline{E}_i\overline{\varepsilon}_{jk}\\ &+\frac{1}{2}\overline{G}_{ijklmn}\overline{\nabla\varepsilon}_{ijk}\overline{\nabla\varepsilon}_{lmn} + \overline{F}_{ijkl}\overline{E}_i\overline{\nabla\varepsilon}_{jkl} + \overline{M}_{ijklm}\overline{\varepsilon}_{ij}\overline{\nabla\varepsilon}_{klm}\\ &-\overline{T}_{ijk}\overline{E}_i\overline{\nabla E}_{jk} - \overline{K}_{ijkl}\overline{\varepsilon}_{ij}\overline{\nabla E}_{kl} - \frac{1}{2}\overline{L}_{ijkl}\overline{\nabla E}_{ij}\overline{\nabla E}_{kl} - \overline{H}_{ijklm}\overline{\nabla E}_{ij}\overline{\nabla\varepsilon}_{klm}.\end{aligned} \tag{1}$$

In Eq. (1), $\overline{C}$, $\overline{\alpha}$, and $\overline{e}$ denote the effective forth-order elastic, second-order dielectric, and third-order piezoelectric tensors, respectively. The term $\overline{F}$ denotes the effective fourth-order flexoelectric tensor, while $\overline{M}$ and $\overline{G}$ correspond to higher order strain gradient elastic tensors (see Ref. 32). The term $\overline{K}$ is the so-called converse flexoelectric tensor.

We note that there are several new coupling tensors in the above energy density expression, whose interpretation is as follows: $\overline{T}$ denotes the relation between an additional polarization (electric field) and an electric field gradient; $\overline{L}$ denotes the relation between a polarization gradient (or electric field gradient) and an electric field gradient, and $\overline{H}$ denotes the relation between a polarization gradient (or electric field gradient) and a strain gradient. A similar expression has also been provided in Ref. 30.

The effective stress tensor $\overline{\sigma}$, effective electric displacement $\overline{d}$, effective hyperstress tensor $\overline{S}$, and hyper-electric displacement $\overline{P}$ associated with the energy density function (1) are defined as

$$\overline{\sigma}_{ij} = \frac{\partial\overline{W}}{\partial\overline{\varepsilon}_{ij}}, \quad \overline{d}_i = -\frac{\partial\overline{W}}{\partial\overline{E}_i}, \quad \overline{S}_{ijk} = \frac{\partial\overline{W}}{\partial\overline{\nabla\varepsilon}_{ijk}}, \quad \overline{P}_{ij} = -\frac{\partial\overline{W}}{\partial\overline{\nabla E}_{ij}}. \tag{2}$$

The corresponding expressions for the stress $\overline{\sigma}$, the electric displacement $\overline{d}$, the hyperstress $\overline{S}$, and hyper-electric displacement $\overline{P}$ are provided by

$$\overline{\sigma}_{ij} = \overline{C}_{ijkl}\overline{\varepsilon}_{kl} - \overline{e}_{kij}\overline{E}_k + \overline{M}_{ijklm}\overline{\nabla\varepsilon}_{klm} - \overline{K}_{ijkl}\overline{\nabla E}_{kl}, \tag{3}$$

$$\overline{d}_i = \overline{e}_{ijk}\overline{\varepsilon}_{jk} + \overline{\alpha}_{ij}\overline{E}_j - \overline{F}_{ijkl}\overline{\nabla\varepsilon}_{jkl} + \overline{T}_{ijk}\overline{\nabla E}_{jk}, \tag{4}$$

$$\overline{S}_{ijk} = \overline{M}_{lmijk}\overline{\varepsilon}_{lm} + \overline{F}_{lijk}\overline{E}_l + \overline{G}_{ijklmn}\overline{\nabla\varepsilon}_{lmn} + \overline{H}_{lmijk}\overline{\nabla E}_{lm}, \tag{5}$$

$$\overline{P}_{ij} = \overline{K}_{klij}\overline{\varepsilon}_{kl} + \overline{T}_{kij}\overline{E}_k - \overline{H}_{ijklm}\overline{\nabla\varepsilon}_{klm} + \overline{L}_{ijkl}\overline{\nabla E}_{kl}. \tag{6}$$

The corresponding equilibrium equations relating these quantities are given by

$$\overline{\sigma}_{ij,j} - \overline{S}_{ijk,jk} = 0, \tag{7}$$

$$\overline{d}_{i,i} - \overline{P}_{ij,ij} = 0. \tag{8}$$

A complete description of boundary conditions for such model can be found in Ref. 33.

III. MICROSCALE EQUATIONS

We consider a periodic composite [see Fig. 1(a)] assumed to be characterized by a 2D representative volume element (RVE) [see Fig. 1(b)]. The RVE is defined in a domain $\Omega \in \mathbb{R}^2$ whose external boundary is denoted by $\partial\Omega$. The characteristic size of the RVE is ℓ. The RVE is subjected to a macroscopic strain $\overline{\boldsymbol{\varepsilon}}$, a macroscopic strain gradient $\overline{\nabla\boldsymbol{\varepsilon}}$, a macroscopic electric field $\overline{\mathbf{E}}$, and a macroscopic electric strain gradient $\overline{\nabla\mathbf{E}}$. The different phases of the material are assumed to be linear piezoelectric and characterized by an elastic tensor $C^{(k)}$, a dielectric tensor $\alpha^{(k)}$, and a piezoelectric tensor $E^{(k)}$, where $k = 1, \ldots, N_p$, with N_p the number of phases. For the

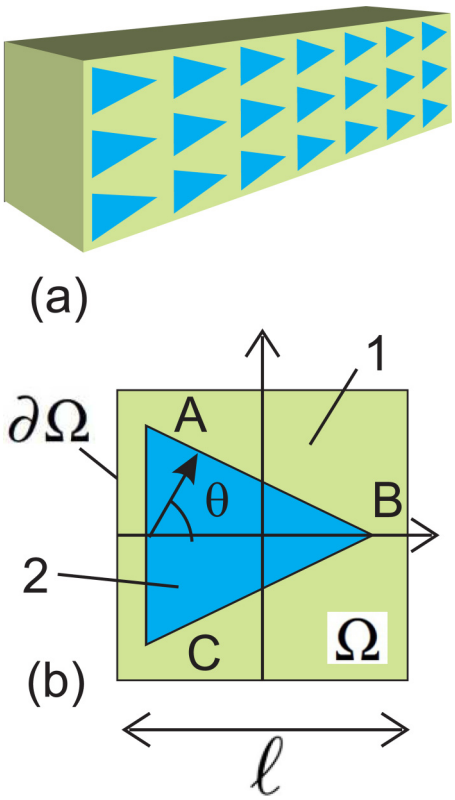

FIG. 1. (a) Periodic piezoelectric structure and (b) representative volume element (RVE). Both matrix (phase 1) and inclusion (phase 2) phases are made of the same piezoelectric material but rotated by a mismatch angle θ.

sake of simplification, we only consider bi-phasic composites ($k = 2$) in the present work. The local equations are given by

$$\sigma_{ij,j} = 0 \text{ in } \Omega, \tag{9}$$

$$d_{i,i} = 0 \text{ in } \Omega, \tag{10}$$

with

$$\sigma_{ij} = C_{ijkl}\varepsilon_{kl} - e_{kij}E_k, \tag{11}$$

$$d_i = e_{ijk}\varepsilon_{jk} + \alpha_{ij}E_j, \tag{12}$$

where $\varepsilon_{ij} = (1/2)(u_{i,j} + u_{j,i})$. Assuming that interfaces between the different material phases are denoted collectively by Γ, we assume perfectly bonded interfacial conditions, i.e.,

$$[[\sigma_{ij}n_j]] = 0, \ \ [[u_i]] = 0 \text{ on } \Gamma, \tag{13}$$

$$[[d_i n_i]] = 0, \ \ [[\phi]] = 0 \text{ on } \Gamma, \tag{14}$$

where $[[\,\cdot\,]]$ denotes the jump across Γ. We define the macroquantities as $\overline{(\cdot)} \equiv \langle\cdot\rangle = (1/V)\int_\Omega (\cdot)dV$ with V being the volume (area in 2D) of Ω. The effective electric field can be computed by prescribing the following electric quadratic boundary conditions over the RVE (see Ref. 20):

$$\phi = -\overline{E}_i x_i - \frac{1}{2}\left(\overline{\nabla E}\right)_{ij} x_i x_j + \tilde{\phi} \text{ on } \partial\Omega, \tag{15}$$

where ϕ is the electric potential such that $E_i = -\phi_{,i}$ and $\tilde{\phi}$ is either zero or a periodic fluctuation on $\partial\Omega$. Mechanical quadratic boundary conditions are introduced to prescribe an effective strain and strain gradient,[34,35]

$$u_i = \overline{\varepsilon}_{ij}x_j + \frac{1}{2}\overline{g}_{ijk}x_j x_k + \tilde{u}_i \text{ on } \partial\Omega, \tag{16}$$

where u_i is a displacement vector related to strain through $\varepsilon_{ij} = \left(u_{i,j} + u_{j,i}\right)$ and

$$\overline{g}_{ijk} = \overline{\nabla\varepsilon}_{ijk} + \overline{\nabla\varepsilon}_{ikj} - \overline{\nabla\varepsilon}_{jki} \tag{17}$$

and $\tilde{u}_i$ is either zero or periodic on $\partial\Omega$. Equations (9) and (10) are completed with the boundary conditions (15) and (16). These equations are here solved by the finite element method (see details in Ref. 20).

It is worth noting that in the case of a homogeneous domain, using (15) and (16) to compute ε_{ij} and E_i and introducing them in Eqs. (9) and (10) does not lead to nonvanishing right-hand terms. This is a well-known issue in the strain gradient homogenization problem, which can cause a dependence to the number of unit cells within the RVE and to nonvanishing higher order properties in the case of materials which do not have local gradient effects (see a discussion in Ref. 32). In our previous work,[36] we have introduced appropriate body forces to balance these nonequilibrated terms. It has also been shown in the context of purely mechanical gradient effects that such procedure is consistent with asymptotic homogenization.[37] However, it has also been discussed in Ref. 32 that such body forces can lead to spurious over predicted effective gradient properties when one of the phases has very low properties. For this reason, we did not adopt this approach in the present paper, which focuses on the development of the homogenization model and on the topology optimization problem. One potential solution to address the above-mentioned issues could be the use of Lagrange multipliers to enforce homogeneous strain gradient and electric field gradients within a homogeneous RVE to extend the method proposed in Ref. 38.

IV. EFFECTIVE TENSORS

The explicit expressions for tensors $\overline{C}$, $\overline{\alpha}$, $\overline{e}$, $\overline{G}$, $\overline{F}$, and $\overline{M}$ can be found in Ref. 20. Following the procedure described in the same reference, the expressions of the new coupling terms including the converse flexoelectric tensor $\overline{K}$ are provided by

$$\overline{T}_{ijk} = \langle B^0_{ipq}C_{pqrs}B^1_{rsjk} - h^0_{ip}e_{pqr}B^1_{qrjk} - B^0_{ipq}e_{pqr}h^1_{rjk} - h^0_{ip}\alpha_{pq}h^1_{qjk}\rangle, \tag{18}$$

$$\overline{K}_{ijkl} = \langle -A^0_{ijpq} C_{pqrs} B^1_{rskl} + D^0_{ijp} e_{pqr} B^1_{qrkl} + A^0_{ijpq} e_{pqr} h^1_{rkl} + D^0_{ijp} \alpha_{pq} h^1_{qkl} \rangle, \tag{19}$$

$$\overline{L}_{ijkl} = \langle B^1_{ijpq} C_{pqrs} B^1_{rskl} - 2h^1_{ijp} e_{pqr} B^1_{qrkl} - h^1_{ijp} \alpha_{pq} h^1_{qkl} \rangle, \tag{20}$$

$$\overline{H}_{ijklm} = \langle -B^1_{ijpq} C_{pqrs} A^1_{rsklm} + B^1_{ijpq} \mathcal{E}_{pqr} D^1_{rklm} + h^1_{ijp} e_{pqr} A^1_{qrklm} + h^1_{ijp} \alpha_{pq} D^1_{qklm} \rangle. \tag{21}$$

In the above equations, the fields B^0, B^1, h^0, h^1, D^0, D^1, A^0, and A^1 are local fields that are obtained by solving the RVE problems (9)–(16) by finite elements. The definition for these tensors can be found in Ref. 20 and are provided for convenience in the supplementary material.

The strong strain or electric field localizations within the medium due to the heterogeneities may lead to a violation of the small perturbation assumption in realistic applications. In that case, extensions to nonlinear formulations of flexoelectricity are available in the literature (see Refs. 39 and 40). However, in the nonlinear case, the effective properties depend on the local fields and identifying the related models can be challenging. Even though this task is out of the scope of this paper, possible strategies for this purpose could rely on data-driven approaches based on artificial intelligence, such as in Refs. 41 and 42.

V. SIMP TOPOLOGY OPTIMIZATION FOR CONVERSE FLEXOELECTRIC COMPOSITES

In this section, we formulate the topology optimization problem to maximize the absolute values of the converse flexoelectric tensor components in (19). First, the periodic unit cell is discretized with a regular mesh of N_e four-node quadrilateral finite elements. We define the inclusion material density ρ_e in each element e, $e = 1, 2, \ldots, N_e$, such that $\rho_e = 1$ is associated with the inclusion phase and $\rho = 0$ is associated with the matrix phase. The topology optimization is formulated as follows:

$$\begin{array}{rc} \text{Maximize}: & |\overline{K}_{ijkl}(\boldsymbol{\rho})| \\ \text{subject}: & \mathbf{KU} = \mathbf{F} \\ : & \sum_{e=1}^{N_e} \rho_e v_e / (\sum_{e=1}^{N_e} v_e) = f \\ & 0 \le \rho_e \le 1, \quad e = 1, 2, \ldots, N_e, \end{array} \tag{22}$$

where $\mathbf{KU} = \mathbf{F}$ is the discrete system obtained when discretizing Eqs. (9)–(16) by the finite element method (see details in Ref. 20). In the above equation, v_e is the volume of an element e and f is the inclusion volume fraction.

We use the SIMP (Solid Isotropic Material with Penalization) method[43–45] to solve the problem. In this framework, the local material properties are interpolated with respect to the local density in a continuous manner, using penalty exponents to enforce local densities to converge to values close to 0 or 1. For composites made of two phases, we use following expressions:

$$\begin{aligned} [C_{ijkl}(\rho)] &= \rho^{pc}[C^2_{ijkl}] + (1-\rho^{pc})[C^1_{ijkl}], \\ [\alpha_{ij}(\rho)] &= \rho^{pa}[\alpha^2_{ij}] + (1-\rho^{pa})[\alpha^1_{ij}], \\ [e_{kij}(\rho)] &= \rho^{pe}[e^2_{kij}] + (1-\rho^{pe})[\mathcal{E}^2_{kij}], \end{aligned} \tag{23}$$

where the superscripts 1 and 2 are associated with matrix and inclusion phases, respectively, and pc, pa, and pe are penalty exponents. In the numerical examples, these values are chosen as $pc = pa = pe = 3$.

The above problem (22) requires evaluating the gradient of the objective function with respect to the local densities (subsequently referred to as sensitivities). The adjoint method has been widely used for sensitivity analysis of gradient-based optimization algorithm[46,47] and is also employed here. The corresponding Lagrangian function for the optimization problem (22) is formed by introducing an adjoint vector $\boldsymbol{\lambda}$ as

$$L = \overline{K}_{ijkl} + \boldsymbol{\lambda} \cdot (\mathbf{KU} - \mathbf{F}), \tag{24}$$

where $\mathbf{KU} - \mathbf{F} = \mathbf{0}$ holds for arbitrary adjoint vectors $\boldsymbol{\lambda}$. Differentiating the Lagrangian function L with respect to the design variable ρ, we have

$$\frac{\partial L}{\partial \rho} = \frac{\partial \overline{K}_{ijkl}}{\partial \rho} + \boldsymbol{\lambda} \cdot \frac{\partial (\mathbf{KU} - \mathbf{F})}{\partial \rho}. \tag{25}$$

The detailed expression can be found following the procedure described in our previous work on the topology optimization of direct flexoelectric properties.[36] The optimization problem (22) is solved by the conservative convex separable approximations (CCSAs) optimizer[48] based on the adjoint sensitivity.

VI. NUMERICAL INVESTIGATIONS

A. Composite with the piezoelectric phase

In this section, we investigate through numerical simulations the significance of the converse flexoelectric and other higher order electromechanical coupling terms in a piezoelectric composite. The geometry of the RVE is depicted in Fig. 1(b), and the triangular inclusion is chosen so as to increase the strain and polarization gradient effects. The characteristic size of the RVE is $\ell = 1$ mm. The position of points A, B, and C in Fig. 1(b) is defined according to $A = \{-a; a\}$, $B = \{a; 0\}$, and $C = \{-a; -a\}$ with $a = \ell\sqrt{0.8\ell}/2$ and corresponds to a volume fraction of inclusions equal to $f = 0.4$. Each phase is made of lead zirconium titanate (PZT) ceramics, but the main orientation of the crystal in both phases is rotated by a mismatch angle $\theta \in [0, 2\pi]$ to create a heterogeneity. The matrix and inclusion phases are denoted by the superscripts 1 and 2, respectively, in Fig. 1(b) and in the following equations. The mechanical, dielectric, and piezoelectric properties

of the PZT matrix phase are given in this 2D configuration by[49,50]

$$[C^1] = \begin{bmatrix} 131.39 & 83.237 & 0 \\ 83.237 & 154.837 & 0 \\ 0 & 0 & 35.8 \end{bmatrix} (\text{GPa}), \tag{26}$$

$$[\alpha^1] = \begin{bmatrix} 2.079 & 0 \\ 0 & 4.065 \end{bmatrix} (\text{C}\,m^{-2}), \tag{27}$$

$$[e^1] = \begin{bmatrix} -2.120582 & -2.120582 & 0 \\ 0 & 0 & 0 \end{bmatrix} (\text{nC}\,m^{-1}\,V^{-1}). \tag{28}$$

The properties of the inclusion phase are defined with respect to the angle θ according to

$$\alpha^2_{ij} = R_{ip}R_{jq}\alpha^1_{pq}, \tag{29}$$

$$e^2_{ijk} = R_{ip}R_{jq}R_{kr}e^1_{pqr}, \tag{30}$$

$$C^2_{ijkl} = R_{ip}R_{jq}R_{kr}R_{ls}C^1_{pqrs}, \tag{31}$$

with

$$R = \begin{bmatrix} \cos(\theta) & -\sin(\theta) \\ \sin(\theta) & \cos(\theta) \end{bmatrix}. \tag{32}$$

In Fig. 2(a), we compute the evolution of the components of the converse flexoelectric tensor $\overline{K}$ with respect to the mismatch angle θ. The values are normalized with respect to the flexoelectric component F_{1221} of PZT to evaluate their significance. We can notice that the components $\overline{K}_{1111}$, $\overline{K}_{1112}$, $\overline{K}_{2211}$, and $\overline{K}_{1212}$ are of the same order (or higher) than the direct flexoelectric coefficients of its constituents for almost all mismatch angles. The components $\overline{K}_{1111}$, $\overline{K}_{2211}$, and $\overline{K}_{1212}$ exhibit an extremum of $0.1860 \times 10^{-3}\,\text{C}\,\text{m}^{-1}$,

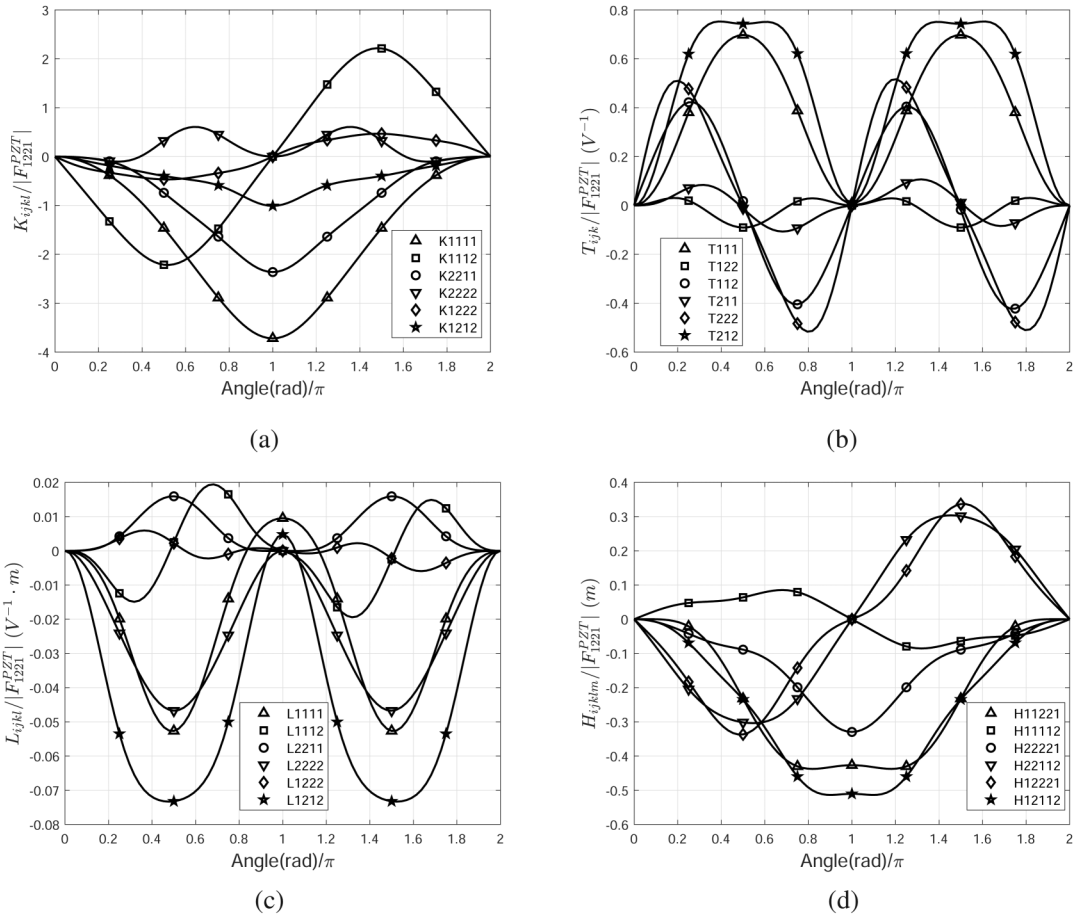

FIG. 2. Evolution of the components of the effective converse flexoelectric tensor: (a) $\overline{K}$, (b) higher order electromechanical coupling term $\overline{T}$, (c) $\overline{L}$, and (d) $\overline{H}$ with respect to the mismatch angle in the piezoelectric composite with triangular inclusions. (a) Evolution of $\overline{K}$ tensor components, (b) evolution of $\overline{T}$ tensor components, (c) evolution of $\overline{L}$ tensor components, and (d) evolution of $\overline{H}$ tensor components.

$0.1181 \times 10^{-3}\,\mathrm{C\,m^{-1}}$, and $0.0504 \times 10^{-3}\,\mathrm{C\,m^{-1}}$, respectively, around $\theta = \pi$, while for $\overline{K}_{1112}$ this extremum is $0.111 \times 10^{-3}\,\mathrm{C\,m^{-1}}$ around $\theta = \pi/2, 3\pi/2$. These results clearly demonstrate that the converse flexoelectric coefficients in piezoelectric composites can make an important contribution to the electromechanical response of the structure and cannot be ignored.

The evolution of the components of the other higher order electromechanical terms $\overline{T}$, $\overline{L}$, and $\overline{H}$ with respect to the mismatch angle θ are computed and shown in Figs. 2(b)–2(d), respectively. Here again, these values are normalized with respect to the flexoelectric properties of PZT to evaluate their significance. The extremum of components $\overline{T}_{111}$, $\overline{T}_{222}$, $\overline{T}_{112}$, and $\overline{T}_{212}$ is comparable to the direct flexoelectric coefficient of PZT. For $\overline{H}$, the extrema of the components $\overline{H}_{11221}$, $\overline{H}_{12112}$, $\overline{H}_{22112}$, and $\overline{H}_{12221}$ are close to the half of the direct flexoelectric coefficient of PZT. However, the effective tensor $\overline{L}$ has much smaller component values as compared to local flexoelectric properties and only plays a negligible role here. Therefore, these results demonstrate that the higher order electromechanical terms $\overline{H}$ and $\overline{T}$ can make a significant contribution to the electromechanical response of piezoelectric composites. More specifically, the coefficients $\overline{T}_{ijk}$ are associated with additional polarization/electric displacement induced by the electric field gradient and thus characterize the importance of these additional effects on the flexoelectric behavior. Taking these new terms into account in the modeling and simulation of flexoelectric structures may help us to design new flexoelectric-based sensors and actuators based on the mechanical and electrical gradient effects.

B. Topology optimization of the ceramic/ceramic piezoelectric composite

Having established that the converse flexoelectric effect makes a significant contribution to the overall flexoelectric response of the PZT/PZT composites, we now perform topology optimization to determine topologies that maximize the converse flexoelectric contributions. We thus consider the topology optimization of a two-phase composite made of piezoelectric phases. Each phase is made with lead zirconium titanate (PZT) ceramics as in the previous example. Here, the crystal lattice is oriented by a mismatch angle of $\theta = \pi$ in the inclusion phase. Then, via (31) and (32), the properties of the inclusion phase can be obtained as $[C^2] = [C^1]$ given by (26), $[\alpha^2] = [\alpha^1]$ given by (27), and

$$[e^2] = \begin{bmatrix} 2.120582 & 2.120582 & 0 \\ 0 & 0 & 0 \end{bmatrix} (\mathrm{nC}\,m^{-1}\,V^{-1}). \tag{33}$$

We perform the topology optimization of the inclusion shape with respect to the converse flexoelectric coefficients $\overline{K}_{1111}$, $\overline{K}_{2211}$, and $\overline{K}_{1212}$ and set the inclusion volume fraction to $f = 0.4$. As a first guess, the design variables are uniformly set to $\rho_e = 0.4$ ($e = 1, \ldots, Ne = 6400$). The guess design with triangular shape which is illustrated in Fig. 1(b) has been investigated in Sec. VI A, recalling that the reference solutions are taken as the extremum values of $\overline{K}_{1111}$, $\overline{K}_{2211}$, and $\overline{K}_{1212}$ for the triangular microstructure at $\theta = \pi$ in Fig. 2(a) and will serve as a comparison solution with respect to optimized topological designs, i.e., $\overline{K}^{\mathrm{ref}}_{1111} = 0.1860 \times 10^{-3}\,\mathrm{C\,m^{-1}}$, $\overline{K}^{\mathrm{ref}}_{2211} = 0.1181 \times 10^{-3}\,\mathrm{C\,m^{-1}}$, and $\overline{K}^{\mathrm{ref}}_{1212} = 0.0504 \times 10^{-3}\,\mathrm{C\,m^{-1}}$. However, for the components $\overline{K}_{1112}$, $\overline{K}_{2222}$, and $\overline{K}_{1222}$, the reference solutions obtained by microstructure with triangular inclusion are all zero at $\theta = \pi$, as shown in Fig. 2(a). Therefore, we do not consider topology optimization for those components in the present case of PZT/PZT composites.

The final optimized unit cell topologies are shown in Fig. 3, where the copper and black colors refer to the inclusion and matrix phases, respectively. The iteration histories for $\overline{K}_{1111}$, $\overline{K}_{2211}$, and $\overline{K}_{1212}$ are shown in Fig. 4. It is noted that the present optimization procedure leads to stable and convergent optimal solutions. The final values for the optimized microstructures are $\overline{K}_{1111} = 0.3525 \times 10^{-3}\,\mathrm{C\,m^{-1}}$, $\overline{K}_{2211} = 0.2241 \times 10^{-3}\,\mathrm{C\,m^{-1}}$, and $\overline{K}_{2112} = 0.0955 \times 10^{-3}\,\mathrm{C\,m^{-1}}$, which represent a significant improvement as compared to the reference triangular solutions by a factor of 1.89 for the components $\overline{K}_{1111}$, $\overline{K}_{2211}$, and $\overline{K}_{1212}$. From Fig. 3, we can see that the three optimized unit cells obtained by $\overline{K}_{1111}$, $\overline{K}_{2211}$, and $\overline{K}_{1212}$ have similar topologies. Finally, we note that the optimized microstructures are similar to the ones obtained

FIG. 3. Optimal topology for $\overline{K}$ for the PZT/PZT composite: (a) $\overline{K}_{1111}$, (b) $\overline{K}_{2211}$, and (c) $\overline{K}_{1212}$.

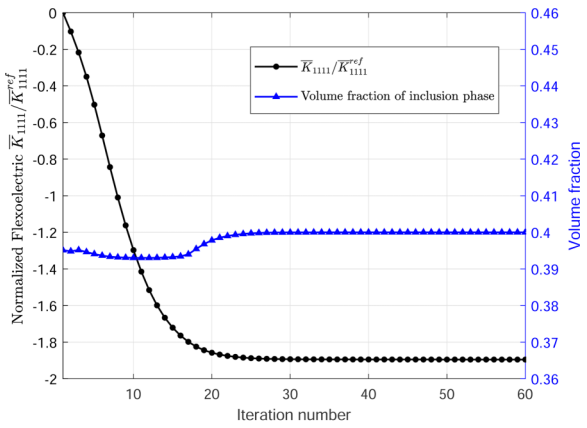

(a)

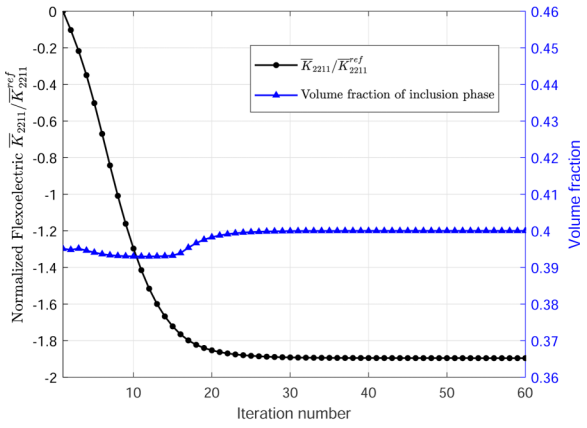

(b)

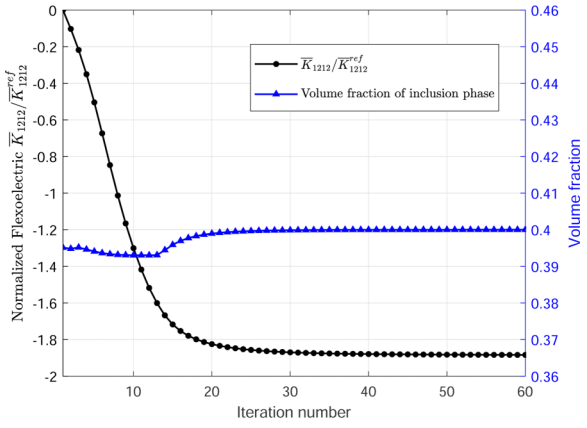

(c)

FIG. 4. Topology optimization process with respect to normalized flexoelectric components and volume fractions for the PZT/PZT composite: (a) $\overline{K}_{1111}$, (b) $\overline{K}_{2211}$, and (c) $\overline{K}_{1212}$.

by optimizing the direct flexoelectric constants $\overline{F}_{1221}$ and $\overline{F}_{2112}$ for the PZT/PZT case.[36]

C. Topology optimization of the ceramic/doped piezoelectric polymer composite

In this example, we replace the stiff PZT inclusion with a soft, dielectric, polymer inclusion (polyvinylidene fluoride, PVDF). The elastic, piezoelectric, and dielectric properties for the polymer are given below. In comparison to the PZT properties, all of the polymer properties are 1–2 orders in magnitude lower than for PZT. The material parameters of matrix PZT are expressed in (26)–(28),[49,50] while the material properties of PVDF are described in (34)–(36),[51]

$$[C^2] = \begin{bmatrix} 6.066 & 3.911 & 0 \\ 3.911 & 6.066 & 0 \\ 0 & 0 & 1.078 \end{bmatrix} (\text{GPa}), \tag{34}$$

$$[\alpha^2] = \begin{bmatrix} 0.025 & 0 \\ 0 & 0.084 \end{bmatrix} (\text{C}\,m^{-2}), \tag{35}$$

$$[e^2] = \begin{bmatrix} 0.1272 & 0.0873 & 0 \\ 0 & 0 & 0 \end{bmatrix} (\text{nC}\,m^{-1}\,V^{-1}). \tag{36}$$

We perform topology optimization of the PVDF inclusion with respect to the converse flexoelectric coefficients $\overline{K}_{1111}$, $\overline{K}_{2211}$, $\overline{K}_{1212}$, $\overline{K}_{2222}$, $\overline{K}_{2212}$, and $\overline{K}_{1211}$. To ensure that these results can be compared against the previous PZT/PZT results, we set the volume fraction of the PVDF inclusion to be $f = 0.4$ for all cases. Similarly, the initial guess is set by $\rho_e = 0.4$, $e = 1, 2, \ldots, Ne = 6400$. The final optimal unit cells of the converse flexoelectric coefficients $\overline{K}_{1111}$, $\overline{K}_{2211}$, $\overline{K}_{1212}$, $\overline{K}_{2222}$, $\overline{K}_{2212}$, and $\overline{K}_{1211}$ are shown in Fig. 5. In these figures, the cyan and black colors refer to the inclusion PVDF and matrix PZT, respectively. The reference solutions calculated by a triangular PVDF inclusion as in Fig. 1(b) are shown for each case. The reference values obtained are $\overline{K}_{1111} = 0.0432 \times 10^{-3}\,\text{C}\,\text{m}^{-1}$, $\overline{K}_{2211} = 0.0139 \times 10^{-3}\,\text{C}\,\text{m}^{-1}$, $\overline{K}_{1212} = 0.0073 \times 10^{-3}\,\text{C}\,\text{m}^{-1}$, $\overline{K}_{2222} = 0.0262 \times 10^{-3}\,\text{C}\,\text{m}^{-1}$, $\overline{K}_{2212} = 0.0033 \times 10^{-3}\,\text{C}\,\text{m}^{-1}$, and $\overline{K}_{1211} = 0.0004 \times 10^{-3}\,\text{C}\,\text{m}^{-1}$ for the PZT/polymer composites with triangular inclusion.

We obtained six different optimized unit cells and a significant improvement can be found as compared to the reference triangular solutions. The optimal absolute values are $\overline{K}_{1111} = 0.3420 \times 10^{-3}\text{C}\,\text{m}^{-1}$, $\overline{K}_{2211} = 0.2054 \times 10^{-3}\text{C}\,\text{m}^{-1}$, $\overline{K}_{1212} = 0.0923 \times 10^{-3}\text{C}\,\text{m}^{-1}$, $\overline{K}_{2222} = 0.1218 \times 10^{-3}\text{C}\,\text{m}^{-1}$, $\overline{K}_{2212} = 0.3267 \times 10^{-3}\text{C}\,\text{m}^{-1}$, and $\overline{K}_{1211} = 0.0821 \times 10^{-3}\text{C}\,\text{m}^{-1}$, which represent increases by factors of 7.92, 14.78, 12.64, 4.65, 99, and 205.25 times, respectively. Interestingly, despite being composed of a polymer inclusion whose (elastic, piezoelectric, and dielectric) properties are all about two orders of magnitude smaller than the PZT matrix, the flexoelectric constants are quite similar to those obtained for the optimized PZT/PZT composites discussed previously, with significantly larger percentage enhancements.

In Figs. 6 and 7, we depict the local electric gradient and strain components of the optimized microstructures that are

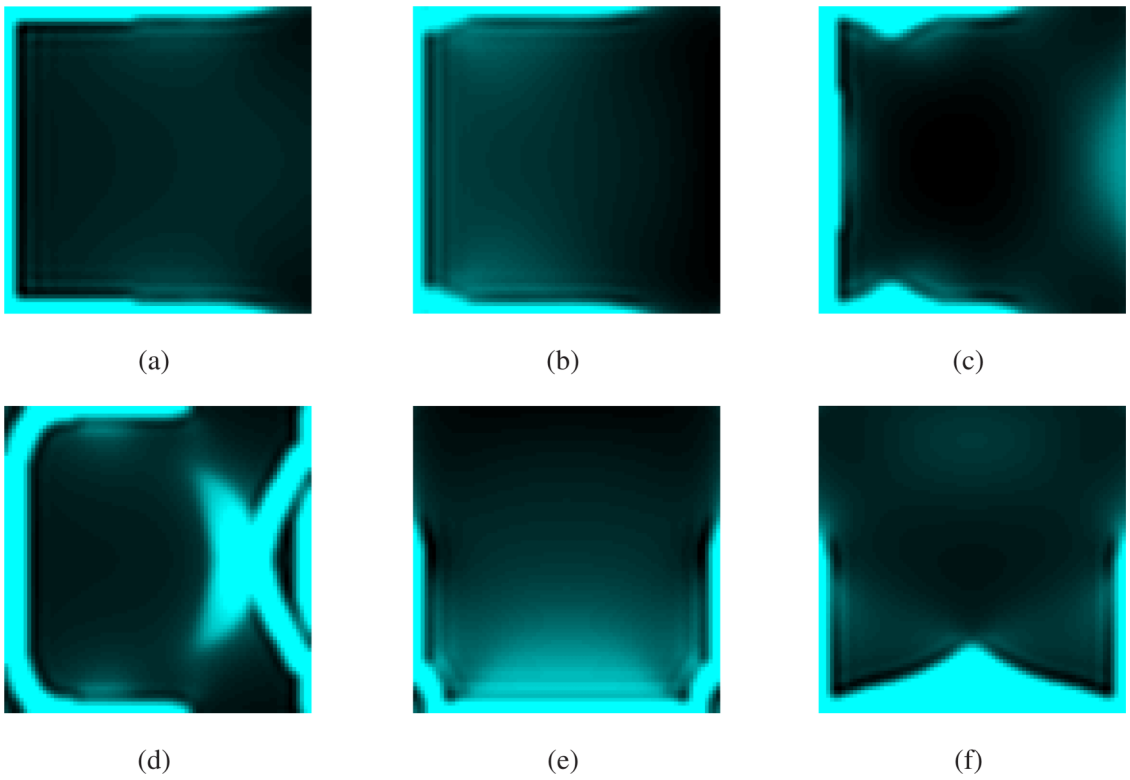

FIG. 5. Optimal topology for $\overline{K}$ for the PZT/PVDF composite: (a) $\overline{K}_{1111}$, (b) $\overline{K}_{2211}$, (c) $\overline{K}_{1212}$, (d) $\overline{K}_{2222}$, (e) $\overline{K}_{2212}$, and (f) $\overline{K}_{1211}$.

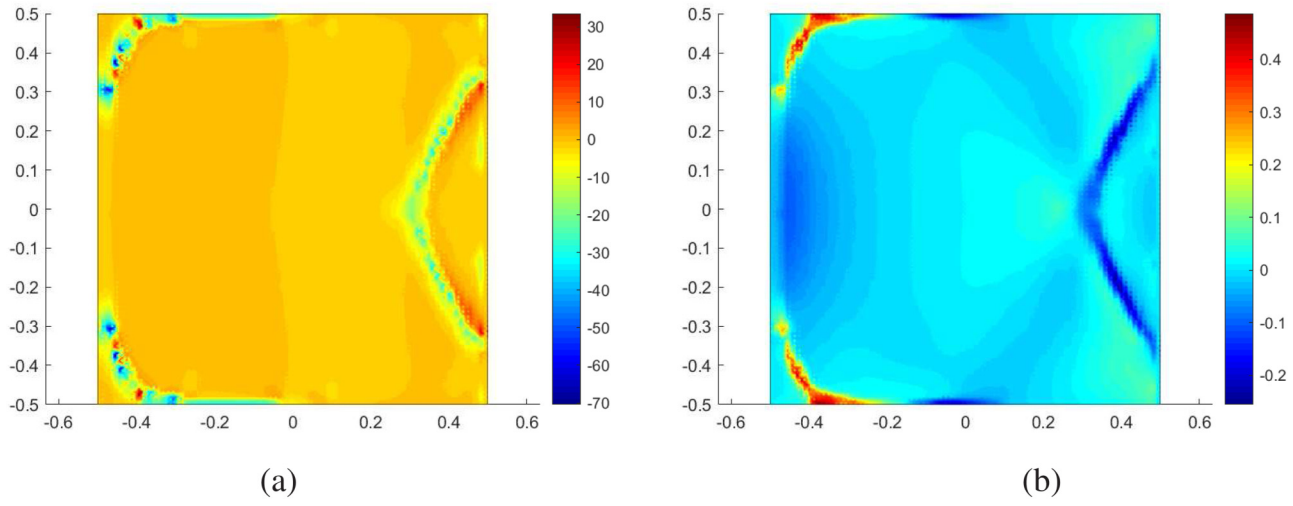

FIG. 6. (a) Electric field gradient component ∇E_{22} and (b) strain component ε_{22} within the PZT-PVDF microstructure corresponding to the optimized coefficient $\overline{K}_{2222}$. (a) Electric gradient ∇E_{22}-component and (b) strain ε_{22}-component.

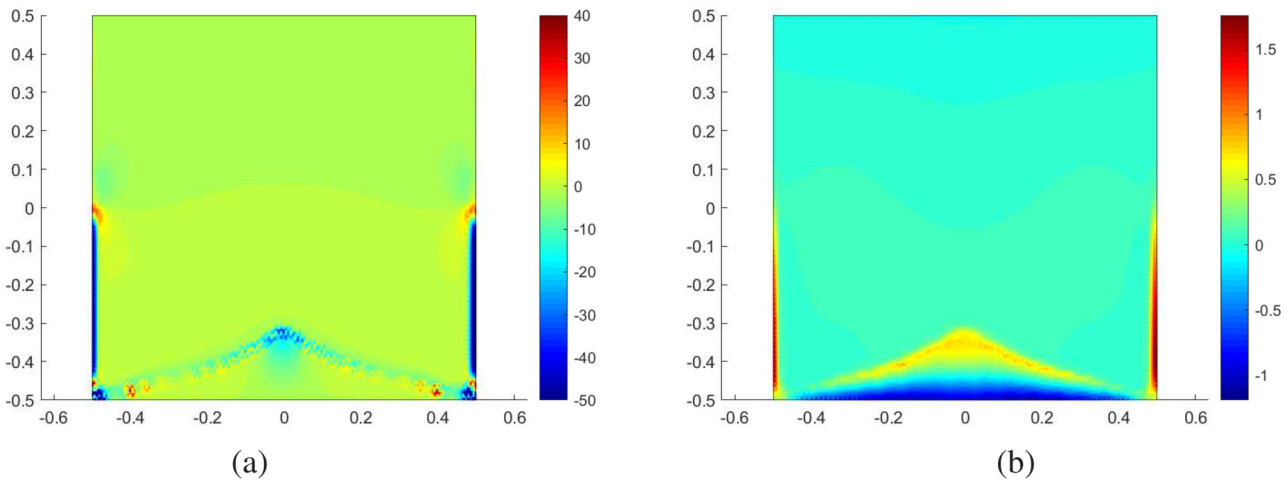

FIG. 7. (a) Electric field gradient component ∇E_{11} and (b) strain component ε_{12} within the PZT-PVDF microstructure corresponding to the optimized coefficient $\overline{K}_{1211}$. (a) Electric gradient ∇E_{11}-component and (b) strain ε_{12}-component.

associated with the converse flexoelectric coefficients $\overline{K}_{2222}$ and $\overline{K}_{1211}$, respectively. In the different cases, we can note that the optimized geometry favors the localization of these fields near the interfaces, which may be expected due to the problem being one of a soft inclusion within a stiff matrix.

VII. CONCLUSIONS

We have proposed an extended flexoelectric model that takes into account not only converse flexoelectric effects but also all other higher order electromechanical coupling terms. A homogenization procedure has been introduced to evaluate numerically these apparent properties in piezoelectric composites. Then, we have combined this model with topology optimization to design microstructures with enhanced converse flexoelectric properties. The numerical investigations revealed that the apparent converse flexoelectric coefficients in a composite made of periodic triangular inclusions have the same order of magnitude as the direct flexoelectric properties of the local constituents. Furthermore, we showed that the other higher order coupling terms, i.e., that relate the electric field to an applied electric field gradient and the strain gradient (bending) to the electric field gradient have non-negligible values as compared to the flexoelectric coefficients. Finally, we show that optimized designs can lead to effective converse flexoelectric properties which can be improved by 1–2 orders of magnitude as compared to guess designs for ceramics/ceramics or polymer/ceramics composites.

SUPPLEMENTARY MATERIAL

See the supplementary material for further details on finite element discretization of the microscale RVE problem and numerical calculation of effective flexoelectric properties.

ACKNOWLEDGMENTS

X.C. and S.Y. gratefully acknowledge the financial support from the National Key R&D Program of China (No. 2016YFB1200602-33), and X.C. acknowledges the funding supported by the Fundamental Research Funds from the Central Universities of Central South University.

DATA AVAILABILITY

The data that support the findings of this study are available from the corresponding author upon reasonable request.

REFERENCES

[1]L. Cross, "Flexoelectric effects: Charge separation in insulating solids subjected to elastic strain gradients," J. Mater. Sci. **41**(1), 53–63 (2006).
[2]J. Y. Fu, W. Zhu, N. Li, and L. Cross, "Experimental studies of the converse flexoelectric effect induced by inhomogeneous electric field in a barium strontium titanate composition," J. Appl. Phys. **100**(2), 024112 (2006).
[3]W. Ma and L. Cross, "Flexoelectric polarization of barium strontium titanate in the paraelectric state," Appl. Phys. Lett. **81**(18), 3440–3442 (2002).
[4]G. Zubko, A. Catalan, P. Buckley, L. Welche, and J. Scott, "Strain-gradient induced polarization in $SrTiO_3$ single crystals," Phys. Rev. Lett. **99**(16), 167601 (2007).
[5]W. Ma and L. Cross, "Strain-gradient induced electric polarization in lead zirconate titanate ceramics," Appl. Phys. Lett. **82**(19), 3923–3925 (2003).
[6]B. Chu and D. Salem, "Flexoelectricity in several thermoplastic and thermosetting polymers," Appl. Phys. Lett. **101**, 103905 (2012).
[7]P. Zubko, G. Catalan, and A. Tagantsev, "Flexoelectric effect in solids," Annu. Rev. Mater. Res. **43**, 387 (2013).
[8]Q. Deng, L. Liu, and P. Sharma, "Flexoelectricity in soft materials and biological membranes," J. Mech. Phys. Solids **62**, 209–227 (2014).
[9]S. Kogan, "Piezoelectric effect during inhomogeneous deformation and acoustic scattering of carriers in crystals," Sov. Phys. Solid State **5**(10), 2069 (1964).
[10]A. K. Tagantsev, "Theory of flexoelectric effect in crystals," Sov. Phys. JETP **61**(6), 1246–1254 (1985).

[11]N. Sharma, C. Landis, and P. Sharma, "Piezoelectric thin-film superlattices without using piezoelectric materials," J. Appl. Phys. **108**, 024304 (2010).
[12]J. Fousek, L. Cross, and D. Litvin, "Possible piezoelectric composites based on the flexoelectric effect," Mater. Lett. **39**, 287–291 (1999).
[13]U. K. Bhaskar, N. Banerjee, A. Abdollahi, Z. Wang, D. G. Schlom, G. Rijnders, and G. Catalan, "A flexoelectric microelectromechanical system on silicon," Nat. Nanotechnol. **11**, 263–266 (2016).
[14]R. Maranganti, N. Sharma, and P. Sharma, "Electromechanical coupling in nonpiezoelectric materials due to nanoscale nonlocal size effects: Greens function solutions and embedded inclusions," Phys. Rev. B **74**, 014110 (2006).
[15]N. Sharma, R. Maraganti, and P. Sharma, "On the possibility of piezoelectric nanocomposites without using piezoelectric materials," J. Mech. Phys. Solids **55**, 2328–2350 (2007).
[16]M. Majdoub, P. Sharma, and T. Cagin, "Enhanced size-dependent piezoelectricity and elasticity in nanostructures due to the flexoelectric effect," Phys. Rev. B **77**, 125424 (2008).
[17]Q. Deng, M. Kammoun, A. Erturk, and P. Sharma, "Nanoscale flexoelectric energy harvesting," Int. J. Solids Struct. **51**, 3218–3225 (2014).
[18]X. Liang, R. Zhang, S. Hu, and S. Shen, "Flexoelectric energy harvesters based on Timoshenko laminated beam theory," J. Intell. Mater. Syst. Struct. **28**, 2064–2073 (2017).
[19]W. Huang, X. Yan, S. R. Kwon, S. Zhang, F.-G. Yuan, and X. Jiang, "Flexoelectric strain gradient detection using $Ba_0.64Sr_0.36TiO_3$ for sensing," Appl. Phys. Lett. **101**, 252903 (2012).
[20]J. Yvonnet, X. Chen, and P. Sharma, "Apparent flexoelectricity due to heterogeneous piezoelectricity," J. Appl. Mech. **87**, 1–31 (2020).
[21]Y. Wang, Y. Tang, Y. Zhu, Y. Feng, and X. Ma, "Converse flexoelectricity around ferroelectric domain walls," Acta Mater. **191**, 158–165 (2020).
[22]X. Tian, M. Xu, Q. Deng, J. Sladek, V. Sladek, M. Repka, and Q. Li, "Size-dependent direct and converse flexoelectricity around a micro-hole," Acta Mech. **231**, 4851–4865 (2020).
[23]A. Abdollahi, N. Domingo, I. Arias, and G. Catalan, "Converse flexoelectricity yields large piezoresponse force microscopy signals in non-piezoelectric materials," Nat. Commun. **10**, 1–6 (2019).
[24]S. Zhang, K. Liu, X. Wen, T. Wu, M. Xu, and S. Shen, "Converse flexoelectricity with relative permittivity gradient," Appl. Phys. Lett. **114**, 052903 (2019).
[25]Z. Shen and W. Chen, "Converse flexoelectric effect in comb electrode piezoelectric microbeam," Phys. Lett. A **376**, 1661–1663 (2012).
[26]L. Shu, W. Huang, S. Ryung Kwon, Z. Wang, F. Li, X. Wei, S. Zhang, M. Lanagan, X. Yao, and X. Jiang, "Converse flexoelectric coefficient f_{1212} in bulk $Ba_{0.67}Sr_{0.33}TiO_3$," Appl. Phys. Lett. **104**, 232902 (2014).
[27]L. Shu, F. Li, W. Huang, X. Wei, X. Yao, and X. Jiang, "Relationship between direct and converse flexoelectric coefficients," J. Appl. Phys. **116**, 144105 (2014).
[28]E. Bursian and O.I. Zaikovskii, "Changes in curvature of a ferroelectric film due to polarization," Sov. Phys. Solid State, USSR **10**, 1121 (1968).
[29]W. Zhu, J. Y. Fu, N. Li, and L. Cross, "Piezoelectric composite based on the enhanced flexoelectric effects," Appl. Phys. Lett. **89**, 192904 (2006).
[30]N. Mawassy, H. Reda, J.-F. Ganghoffer, V. Eremeyev, and H. Lakiss, "A variational approach of homogenization of piezoelectric composites towards piezoelectric and flexoelectric effective media," Int. J. Eng. Sci. **158**, 103410 (2021).
[31]B. Wang, Y. Gu, S. Zhang, and L.-Q. Chen, "Flexoelectricity in solids: Progress, challenges, and perspectives," Prog. Mater. Sci. **106**, 100570 (2019).
[32]J. Yvonnet, N. Auffray, and V. Monchiet, "Computational second-order homogenization of materials with effective anisotropic strain gradient behavior," Int. J. Solids Struct. **191–192**, 434–448 (2020).
[33]S. Sidhardh and M. Ray, "Exact solutions for flexoelectric response in elastic dielectric nanobeams considering generalized constitutive gradient theories," Int. J. Mech. Mater. Des. **15**, 427–446 (2019).
[34]M. Gologanu, J.-B. Leblond, G. Perrin, and J. Devaux, "Recent extensions of Gurson's model for porous ductile metals," in *Continuum Micromechanics* (Springer, 1997), pp. 61–130.
[35]S. Forest, "Mechanics of generalized continua: Construction by homogenizaton," J. Phys. IV **8**, Pr4–Pr39 (1998).
[36]X. Chen, J. Yvonnet, S. Yao, and H. Park, "Topology optimization of flexoelectric composites using computational homogenization," Comput. Methods Appl. Mech. Eng. **381**, 113819 (2021).
[37]V. Monchiet, N. Auffray, and J. Yvonnet, "Strain-gradient homogenization: A bridge between asymptotic expansion and quadratic boundary condition methods," Mech. Mater. **143**, 103309 (2020).
[38]L. Kaczmarczyk, C. Pearce, and N. Bićanić, "Scale transition and enforcement of RVE boundary conditions in second-order computational homogenization," Int. J. Numer. Methods Eng. **74**, 506–522 (2008).
[39]L. Liu, "An energy formulation of continuum magneto-electro-elasticity with applications," J. Mech. Phys. Solids **63**, 451–480 (2014).
[40]J. Yvonnet and L. Liu, "A numerical framework for modeling flexoelectricity and Maxwell stress in soft dielectrics at finite strains," Comput. Methods Appl. Mech. Eng. **313**, 450–482 (2017).
[41]X. Lu, D. Giovanis, J. Yvonnet, V. Papadopoulos, F. Detrez, and J. Bai, "A data-driven computational homogenization method based on neural networks for the nonlinear anisotropic electrical response of graphene/polymer nanocomposites," Comput. Mech. **64**, 307–321 (2019).
[42]B. Le, J. Yvonnet and Q.-C. HE, "Computational homogenization of nonlinear elastic materials using neural networks," Int. J. Numer. Methods Eng. **104**, 1061–1084 (2015).
[43]M. P. Bendsøe, "Optimal shape design as a material distribution problem," Struct. Optim. **1**, 193–202 (1989).
[44]G. I. Rozvany, M. Zhou, and T. Birker, "Generalized shape optimization without homogenization," Struct. Optim. **4**, 250–252 (1992).
[45]M. P. Bendsøe and O. Sigmund, "Material interpolation schemes in topology optimization," Arch. Appl. Mech. **69**, 635–654 (1999).
[46]V. Komkov, K. Choi, and E. Haug, *Design Sensitivity Analysis of Structural Systems*, Mathematics in Science and Engineering (Elsevier Science, 1986).
[47]M. P. Bendsøe and O. Sigmund, *Topology Optimization: Theory, Methods, and Applications*, 2nd ed. (Springer, 2013), p. 381.
[48]K. Svanberg, "A class of globally convergent optimization methods based on conservative convex separable approximations," SIAM J. Optim. **12**, 555–573 (2002).
[49]E. Pettermann and S. Suresh, "A comprehensive unit cell model: A study of coupled effects in piezoelectric 1–3 composites," Int. J. Solids Struct. **37**, 5447–5464 (2000).
[50]R. Brenner, "Numerical computation of the response of piezoelectric composites using Fourier transform," Phys. Rev. B **79**, 184106 (2009).
[51]K. S. Ramadan, D. Sameoto, and S. Evoy, "A review of piezoelectric polymers as functional materials for electromechanical transducers," Smart Mater. Struct. **23**, 033001 (2014).